

Properties of the mixed phase core in maximum mass neutron stars

Xuhao Wu,^{1,*} Peng-Cheng Chu,^{2,3,†} Min Ju,^{4,‡} and He Liu^{2,3,§}

¹*Key Laboratory for Microstructural Material Physics of Hebei Province,
School of Science, Yanshan University, Qinhuangdao, 066004, China*

²*Science School, Qingdao University of Technology, Qingdao 266000, China*

³*The Research Center of Theoretical Physics, Qingdao University of Technology, Qingdao 266033, China*

⁴*College of Science, China University of Petroleum (East China), Qingdao 266580, China*

In the context of observed massive neutron stars (NSs), we examine the internal structure, phase transitions, and the impacts of the equation of state (EOS) in maximum NSs. We investigate the stiffness changes in the EOS during the hadron-quark phase transition within the NSs. The relativistic mean-field (RMF) model and RMF model with a density-dependent isovector coupling, known as the RMFL model, are used to describe hadronic matter, while to the represent quark matter, the Nambu-Jona-Lasinio (NJL) model is applied. We explore the strength of vector coupling in quark matter, which delayed the onset density and reduced the maximum mass of NS, but does not exhibit a clear correlation with the NS central density. A considerable size of the mixed phase core could exist in the maximum mass NS but with corresponding small mixed phase mass.

I. INTRODUCTION

The equation of state (EOS) plays a crucial role in the fields of nuclear physics and astrophysics [1], as it determines the composition and properties of compact stars. It also sheds light on the nature of strong interactions within these stars. The quantum chromodynamics (QCD) phase transition at finite temperature and low baryon density support the hot dense quark matter exist, while cold dense quark matter may only can found in neutron stars (NS). The question of whether quark matter can exist in NSs has been a topic of interest for researchers for several decades [2, 3], yet it remains an open question. At high density, there is a Bodmer–Witten assumption that strange quark matter composed of uds quarks may actually be the true ground state of matter [4], exhibiting a lower energy per baryon compared to both ud quark matter and nucleon matter. Whether strange quark matter is absolutely stable is model dependent [5]. Overall, it is possible that a first-order hadron-quark phase transition occurs within the core of massive NS [6–8], where the density could reach $5 \sim 10$ times saturation density n_0 .

In the past decade, significant progress in astronomical observations has provided abundant data on neutron star mass, radius, and tidal deformabilities. These constraints have spurred explorations into theories of dense matter, narrowing down the range of plausible strong interaction theories. Recent Shapiro delay measurements of massive neutron star PSR J0740+6620 [9, 10], gives a lower limit of $2.14^{+0.10}_{-0.09} M_\odot$ (68.3% credibility inter-

val), similar restrictions are also imposed by PSR J1614-2230 ($1.908 \pm 0.016 M_\odot$) [11] and PSR J0348+0432 ($2.01 \pm 0.04 M_\odot$) [12], respectively. These results provides constraints on the EOSs, that disallow configurations unable to support twice the solar mass. Additionally, the black-widow pulsar, PSR J0952-0607, reports a mass of $2.35 \pm 0.17 M_\odot$ [13] (68.3% credibility interval), which is the heaviest NS observed. The inferred mass M and equatorial radius R from x-ray data detected with the Neutron Star Interior Composition Explorer (NICER) view of PSR J0030+0451 suggested estimation are (68% credible interval) $M = 1.34^{+0.15}_{-0.16} M_\odot$, $R = 12.71^{+1.14}_{-1.19}$ km [14] as well as $M = 1.44^{+0.15}_{-0.14} M_\odot$, $R = 13.02^{+1.24}_{-1.06}$ km [15], respectively. Moreover, NICER view observations of PSR J0740+6620 (68.3% credibility interval) suggest a mass of $M = 2.072^{+0.067}_{-0.066} M_\odot$, $R = 12.39^{+1.30}_{-0.98}$ km [16] and $M = 2.08 \pm 0.07 M_\odot$, $R = 13.7^{+2.6}_{-1.5}$ km [17]. These massive NS ruled out the soft EOSs. The possibility that the secondary component of the gravitational wave event GW190814 may be the most massive NS [18] or a black hole. The GW170817 event provided constraints on tidal deformations $\Lambda < 800$ [19]. A roughly $1.4 M_\odot$ NS radius, consistent with the tidal deformability up limit, refers $R_{1.4} \leq 13.6$ km [20]. The NICER and gravitational wave detection have opened new avenues for exploration.

On one hand, the massive NS mass constraints need stiff EOS, on the other hand, the radius or tidal deformability limit need relative soft EOS in low-density range. To fulfil these constraints above, many works contain quark degree of freedom in NS have been done [5, 21–26]. A relative large pure quark core in the massive NS is expected in Ref. [23] using speed-of-sound interpolation between chiral effective field theory (CET) and perturbative-QCD (pQCD) EOSs. This conclusion is supported in Ref. [21, 22] with additional quark interactions, in which the eight-quark vector interaction and

*Electronic address: wuhaobird@gmail.com

†Electronic address: kyois@126.com

‡Electronic address: jumin@upc.edu.cn

§Electronic address: liuhe@qut.edu.cn

the four-quark isovector-vector interaction play very different roles in determining the size of the quark core. The framework of hybrid star with twin star under Maxwell construction is discussed in Ref. [27, 28]. Ref. [29] raised a model contain sequential phase transitions from hadronic matter to low- and then to high-density quark matter phases. Usually hadron-quark phase transition will not affect the properties of $1.4 M_\odot$ NS properties, since the onset density beyond the central density of $1.4 M_\odot$ NS. But twin star could give another counterpart with smaller radius.

The purpose of this study is explore the stiffness changes in the EOS during the transition from hadronic matter to quark matter, and to investigate the properties of the maximum mass NS containing quark degree of freedom, taking into account the recent observational constraints listed above. Describing both hadronic and quark matter within a unified framework presents challenges, as these phases typically involve different particles. Usually distinct models are required, then select the phase with the lower energy density at given baryon number density. To describe hadronic matter, we employ the relativistic mean-field (RMF) model and RMF model with a density-dependent isovector coupling, like the way in the density-dependent relativistic mean-field (DDRMF) model, refereed as RMFL mdoel [30, 31]. For the representation of quark matter, We apply the Nambu-Jona-Lasinio (NJL) model. The Gibbs construction [3] is adopted for modeling the hadron-quark mixed phase, different from Maxwell construction, which could be considered as a extremely high surface tension that Gibbs construction becomes unstable [32, 33]. In the Gibbs construction both hadronic matter and quark matter could coexist within a density region characterized by dynamic equilibrium, baryon chemical potential equilibrium and global charge neutrality. The transition from the hadronic phase to the quark phase results in a softening of the EOS, leading to a lower maximum mass of NS compared to their pure hadronic counterparts, due to the increase in degrees of freedom. By analyzing these aspects, the study could enhance our understanding of the EOS behavior and characteristics of maximum mass NS with quark matter. In this study, hyperons in the hadronic matter are neglected due to the lack of experimental or observational evidence supporting their presence in compact star cores. Furthermore, the onset density of quarks and hyperons are close which make it complicated to distinguish the effect of hyperons or quarks degree of freedom on EOS and NS properties.

This article is structured as follows. In Section II, we provide a concise overview of the NJL model, which describes quark matter, as well as the RMF/RMFL model, which characterizes hadronic matter. Additionally, the hadron-quark phase transition under Gibbs equilibrium is discussed. In Sec. III, we present the numerical results of the hadron-quark phase transition, and provide a detailed analysis of the events occurring during this process, including its effect on the properties of the max-

imum mass HS. Finally, Section IV offers a summary of our findings.

II. THE THEORETICAL MODEL

A. Hadronic matter phase

The RMF/RMFL model is employed to describe the hadronic matter, where nucleons interact through the exchange of isoscalar-scalar meson σ , isoscalar-vector meson ω , and isovector-vector meson ρ . In the RMF model, the isovector-vector meson coupling g_ρ is a constant, whereas in the RMFL model, it varies with the change of number density n_b . The Lagrangian density for the hadronic matter, comprising nucleons (p and n) and leptons (e and μ) is written as

$$\begin{aligned} \mathcal{L}_{\text{RMF/RMFL}} = & \sum_{i=p,n} \bar{\psi}_i \{i\gamma_\mu \partial^\mu - (M + g_\sigma \sigma) \\ & - \gamma_\mu [g_\omega \omega^\mu + \frac{g_\rho}{2} \tau_a \rho^{a\mu}] \} \psi_i \\ & + \frac{1}{2} \partial_\mu \sigma \partial^\mu \sigma - \frac{1}{2} m_\sigma^2 \sigma^2 - \frac{1}{3} g_2 \sigma^3 - \frac{1}{4} g_3 \sigma^4 \\ & - \frac{1}{4} W_{\mu\nu} W^{\mu\nu} + \frac{1}{2} m_\omega^2 \omega_\mu \omega^\mu + \frac{1}{4} c_3 (\omega_\mu \omega^\mu)^2 \\ & - \frac{1}{4} R_{\mu\nu}^a R^{a\mu\nu} + \frac{1}{2} m_\rho^2 \rho_\mu^a \rho^{a\mu} \\ & + \Lambda_v (g_\omega^2 \omega_\mu \omega^\mu) (g_\rho^2 \rho_\mu^a \rho^{a\mu}) \\ & + \sum_{l=e,\mu} \bar{\psi}_l (i\gamma_\mu \partial^\mu - m_l) \psi_l, \end{aligned} \quad (1)$$

where $W^{\mu\nu}$ and $R^{a\mu\nu}$ denote the antisymmetric field tensors associated with ω^μ and $\rho^{a\mu}$, respectively. Within the RMF/RMFL approach, the meson fields are considered classical fields, and the field operators are substituted with their corresponding expectation values. For a static system, the non-vanishing expectation values are $\sigma = \langle \sigma \rangle$, $\omega = \langle \omega^0 \rangle$, and $\rho = \langle \rho^{30} \rangle$.

In uniform hadronic matter, the equations of motion for meson mean fields can be expressed as

$$m_\sigma^2 \sigma + g_2 \sigma^2 + g_3 \sigma^3 = -g_\sigma (n_p^s + n_n^s), \quad (2)$$

$$m_\omega^2 \omega + c_3 \omega^3 + 2\Lambda_v g_\omega^2 g_\rho^2 \rho^2 \omega = g_\omega (n_p + n_n), \quad (3)$$

$$m_\rho^2 \rho + 2\Lambda_v g_\omega^2 g_\rho^2 \omega^2 \rho = \frac{g_\rho}{2} (n_p - n_n), \quad (4)$$

where n_i^s and n_i denote the scalar and number densities of species i , respectively. In the context of hadronic matter under β equilibrium, the chemical potentials satisfy the relations $\mu_p = \mu_n - \mu_e$ and $\mu_\mu = \mu_e$. At zero temperature approximation, the chemical potentials are given by

$$\mu_i = \sqrt{k_F^i{}^2 + M^{*2}} + g_\omega \omega + g_\rho \tau_3^i \rho, \quad i = p, n, \quad (5)$$

$$\mu_l = \sqrt{k_F^l{}^2 + m_l^2}, \quad l = e, \mu, \quad (6)$$

where $M^* = M + g_\sigma \sigma$ denotes the effective nucleon mass. The energy density of hadronic phase (HP) is expressed as

$$\begin{aligned} \varepsilon_{\text{HP}} = & \sum_{i=p,n} \frac{1}{\pi^2} \int_0^{k_F^i} \sqrt{k^2 + M^{*2}} k^2 dk \\ & + \frac{1}{2} m_\sigma^2 \sigma^2 + \frac{1}{3} g_2 \sigma^3 + \frac{1}{4} g_3 \sigma^4 + \frac{1}{2} m_\omega^2 \omega^2 \\ & + \frac{3}{4} c_3 \omega^4 + \frac{1}{2} m_\rho^2 \rho^2 + 3\Lambda_v (g_\omega^2 \omega^2) (g_\rho^2 \rho^2) \\ & + \sum_{l=e,\mu} \frac{1}{\pi^2} \int_0^{k_F^l} \sqrt{k^2 + m_l^2} k^2 dk, \end{aligned} \quad (7)$$

and the pressure is calculated as

$$\begin{aligned} P_{\text{HP}} = & \sum_{i=p,n} \frac{1}{3\pi^2} \int_0^{k_F^i} \frac{k^4 dk}{\sqrt{k^2 + M^{*2}}} \\ & - \frac{1}{2} m_\sigma^2 \sigma^2 - \frac{1}{3} g_2 \sigma^3 - \frac{1}{4} g_3 \sigma^4 + \frac{1}{2} m_\omega^2 \omega^2 \\ & + \frac{1}{4} c_3 \omega^4 + \frac{1}{2} m_\rho^2 \rho^2 + \Lambda_v (g_\omega^2 \omega^2) (g_\rho^2 \rho^2) \\ & + \sum_{l=e,\mu} \frac{1}{3\pi^2} \int_0^{k_F^l} \frac{k^4 dk}{\sqrt{k^2 + m_l^2}}, \end{aligned} \quad (8)$$

In the RMFL model, $g_\rho(n_b)$ varies with the change in baryon number density n_b ,

$$g_\rho(n_b) = g_\rho(n_0) \exp \left[-a_\rho \left(\frac{n_b}{n_0} - 1 \right) \right], \quad (9)$$

where n_0 is the saturation density. This difference from the constant g_ρ in the RMF model results in a rearrangement item for nucleons in the RMFL model,

$$\Sigma_r = \frac{1}{2} \sum_{i=p,n} \frac{\partial g_\rho(n_b)}{\partial n_b} \tau_3 n_i \rho = -\frac{1}{2} a_\rho g_\rho(n_b) \frac{n_p - n_n}{n_0} \rho, \quad (10)$$

and contributes to the formulation of the chemical potential

$$\mu_p = \sqrt{(k_F^p)^2 + M^{*2}} + g_\omega \omega + \Sigma_r + \frac{g_\rho(n_b)}{2} \rho, \quad (11)$$

$$\mu_n = \sqrt{(k_F^n)^2 + M^{*2}} + g_\omega \omega + \Sigma_r - \frac{g_\rho(n_b)}{2} \rho. \quad (12)$$

The pressure also affected by the rearrangement item Σ_r ,

$$\begin{aligned} P_{\text{HP}} = & \sum_{i=p,n} \frac{1}{3\pi^2} \int_0^{k_F^i} \frac{1}{\sqrt{k^2 + M^{*2}}} k^4 dk \\ & - \frac{1}{2} m_\sigma^2 \sigma^2 - \frac{1}{3} g_2 \sigma^3 - \frac{1}{4} g_3 \sigma^4 + \frac{1}{2} m_\omega^2 \omega^2 \\ & + \frac{1}{4} c_3 \omega^4 + \frac{1}{2} m_\rho^2 \rho^2 + \Lambda_v (g_\omega^2 \omega^2) (g_\rho^2 \rho^2) \\ & + n_b \Sigma_r + \sum_{l=e,\mu} \frac{1}{3\pi^2} \int_0^{k_F^l} \frac{k^4 dk}{\sqrt{k^2 + m_l^2}}, \end{aligned} \quad (13)$$

while the energy density remains unaffected. When a_ρ in Eq. 9 equals zero, the rearrangement term Σ_r vanished, and Eqs. (11-12) simplifies to Eq. (5), the pressure Eq. (13) simplifies to Eq. (8).

In order to investigate the impact of EOS on NS structures and the hadron-quark phase transition, we adopt the successful RMF/RMFL models, including BigApple [34], NL3L-50 [31], TM1e [35, 36] and NL3 [37] to characterize nuclear interactions. The details of NL3L-50 is comprehensively outlined in Ref. [31]. For the sake of completeness, we present the parameter sets and saturation properties of these models in Tables I and II, respectively.

It is well known that nuclear symmetry energy E_{sym} and its slope L play a crucial role in determining the properties of neutron stars. Within the Ref. [38, 39], there are commonly used constraints for these quantities: the symmetry energy E_{sym} lies within the range of $25\text{MeV} < E_{\text{sym}} < 36\text{MeV}$, while the slope L about $L = 57.7 \pm 19 \text{ MeV}$. The parameters adopted in this study fall within the aforementioned range, except NL3, which is concluded as a comparison.

TABLE I: Masses of nucleons and mesons and meson coupling constants. The masses are provided in units of MeV.

Parameters	BigApple	NL3L-50	TM1e	NL3
M	939.0	939.0	938.0	939.0
m_σ	492.730	508.194	511.198	508.194
m_ω	782.500	782.501	783.000	782.501
m_ρ	763.0	763.0	770.0	763.0
g_σ	9.6699	10.217	10.0289	10.217
g_ω	12.316	12.868	12.6139	12.868
g_ρ	14.1618	8.948	12.2413	8.948
g_2/fm^{-1}	11.9214	10.431	7.2325	10.431
g_3	-31.6796	-28.885	0.6183	-28.885
c_3	2.6843	0	71.3075	0
Λ_v	0.0475	0	0.0327	0
a_ρ	0	0.583455	0	0

TABLE II: Saturation properties of symmetric nuclear matter for the BigApple, NL3L-50, TM1e, and NL3 models. The quantities E_0 , K , E_{sym} , and L represent the energy per nucleon, incompressibility coefficient, symmetry energy, and symmetry energy slope at saturation density n_0 , respectively.

Model	n_0 (fm $^{-3}$)	E_0 (MeV)	K (MeV)	E_{sym} (MeV)	L (MeV)
BigApple	0.155	-16.34	227.0	31.3	39.8
NL3L-50	0.148	-16.24	272.3	37.4	50
TM1e	0.145	-16.26	281.0	32.4	50
NL3	0.148	-16.24	272.3	37.4	118.5

B. Quark matter phase

To describe the quark matter, we chose to utilize the SU(3) NJL model, which incorporates three flavors of quarks uds . The Lagrangian density of the NJL model is give by

$$\begin{aligned} \mathcal{L}_{\text{NJL}} = & \bar{q} (i\gamma_\mu \partial^\mu - m^0) q \\ & + G_S \sum_{a=0}^8 \left[(\bar{q} \lambda_a q)^2 + (\bar{q} i\gamma_5 \lambda_a q)^2 \right] \\ & - K \{ \det [\bar{q} (1 + \gamma_5) q] + \det [\bar{q} (1 - \gamma_5) q] \} \\ & - G_V \sum_{a=0}^8 \left[(\bar{q} \gamma^\mu \lambda_a q)^2 + (\bar{q} \gamma^\mu \gamma_5 \lambda_a q)^2 \right], \quad (14) \end{aligned}$$

where q refers to the quark field, which contains three flavors ($N_f = 3$) and three colors ($N_c = 3$). The current quark mass matrix is given by $m^0 = \text{diag}(m_u^0, m_d^0, m_s^0)$. In this study, we take into account chirally symmetric four-quark interaction characterized by the coupling constant G_S , Kobayashi–Maskawa–t Hooft (KMT) six-quark interaction represented by the coupling constant K , and repulsive vector interaction governed by the coupling constant G_V . The inclusion of the vector coupling is essential in describing massive stars, as shown in Refs. [5, 40–43]. In our current study, we adopt the parameters provided in Ref. [44], $m_u^0 = m_d^0 = 5.5$ MeV, $m_s^0 = 140.7$ MeV, $\Lambda = 602.3$ MeV, $G_S \Lambda^2 = 1.835$, and $K \Lambda^5 = 12.36$. The vector coupling G_V is treated as a free parameter in our analysis, following the approach adopted in Refs. [40, 43]. This is because there is currently no well-constrained value for G_V at finite density. By treating G_V as a free parameter, we aim to explore its influence on the properties and behavior of quark matter within our study. Since the vector coupling G_V only serves to stiffen the EOS of quark matter, its effects on the hadron-quark phase transition are expected to be qualitatively similar across different models. By including G_V , the EOS would become more resistant to compression, resulting in increased pressure for a given density.

At the mean-field level, the constituent quark masses arise from spontaneous chiral symmetry breaking. In vacuum, the constituent quark mass m_i^* is much larger than the current quark mass m_i^0 . The determination of constituent quark masses m_i^* in quark matter involves solving the relevant gap equations,

$$m_i^* = m_i^0 - 4G_S \langle \bar{q}_i q_i \rangle + 2K \langle \bar{q}_j q_j \rangle \langle \bar{q}_k q_k \rangle, \quad (15)$$

with (i, j, k) being any permutation of (u, d, s) . The energy density of quark matter is given by

$$\begin{aligned} \varepsilon_{\text{NJL}} = & \sum_{i=u,d,s} \left[-\frac{3}{\pi^2} \int_{k_F^i}^\Lambda \sqrt{k^2 + m_i^{*2}} k^2 dk \right] \\ & + 2G_S (C_u^2 + C_d^2 + C_s^2) - 4KC_u C_d C_s \\ & + 2G_V (n_u^2 + n_d^2 + n_s^2) - \varepsilon_0, \quad (16) \end{aligned}$$

where $C_i = \langle \bar{q}_i q_i \rangle$ denotes the quark condensate of flavor i . The constant ε_0 is introduced to ensure that the energy density ε_{QP} in the physical vacuum is zero. In our current study, the choice of ε_0 lead the pressure also vanishes in the vacuum.

In quark matter, the chemical potentials of quarks and leptons satisfy the β equilibrium condition, which is expressed as $\mu_s = \mu_d = \mu_u + \mu_e$ and $\mu_\mu = \mu_e$. The chemical potential of quark flavor $i = u, d, s$ is given by

$$\mu_i = \sqrt{k_F^i{}^2 + m_i^{*2}} + 4G_V n_i, \quad (17)$$

The total energy density and pressure in quark phase (QP) are written as

$$\varepsilon_{\text{QP}} = \varepsilon_{\text{NJL}} + \sum_{l=e,\mu} \frac{1}{\pi^2} \int_0^{k_F^l} \sqrt{k^2 + m_l^2} k^2 dk, \quad (18)$$

$$P_{\text{QP}} = \sum_{i=u,d,s,e,\mu} n_i \mu_i - \varepsilon_{\text{QP}}. \quad (19)$$

C. Hadron-quark mixed phase

In our study, we employ the Gibbs construction to describe the hadron-quark mixed phase. Within this construction, the system satisfies the β equilibrium is satisfied. Both hadronic matter and quark matter are allowed to be charged separately, but the total charge remains zero. The energy density of the mixed phase (MP) is

$$\varepsilon_{\text{MP}} = u\varepsilon_{\text{QP}} + (1 - u)\varepsilon_{\text{HP}}, \quad (20)$$

where u is the volume fraction of quark matter. The pressure equilibrium and the chemical potential equilibrium between two phases are shown below,

$$P_{\text{HP}} = P_{\text{QP}}, \quad (21)$$

$$\mu_u + \mu_e = \mu_d = \mu_s = \frac{1}{3}\mu_n + \frac{1}{3}\mu_e, \quad (22)$$

At a given baryon density n_b , there are two independent chemical potentials, μ_n and μ_e , which can be determined by the constraints of global charge neutrality and baryon number conservation given in

$$0 = n_e + n_\mu - \frac{u}{3} (2n_u - n_d - n_s) - (1 - u)n_p, \quad (23)$$

$$n_b = \frac{u}{3} (n_u + n_d + n_s) + (1 - u) (n_p + n_n). \quad (24)$$

All properties of the mixed phase can be calculated, under the equilibrium state with given n_b .

III. RESULTS AND DISCUSSION

The presence of deconfined quarks in the core of massive NSs is an intriguing possibility. In this section, we

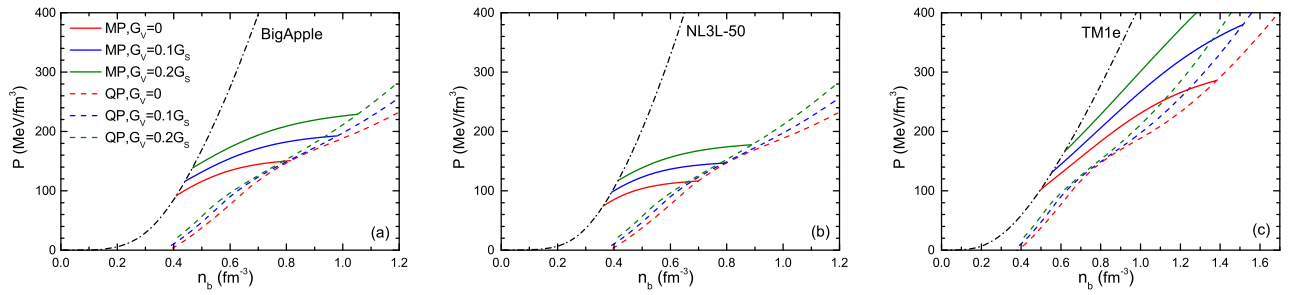


FIG. 1: (Color online) Pressures P as a function of the number density n_b obtained using different parameter sets BigApple, NL3L-50 and TM1e. The results for hadronic phase, the mixed phase (MP), and the quark phase (QP) are represented by dash-dot lines, solid lines and dash lines, respectively. Additionally, the strengths of the vector coupling is varied with $G_V = 0, 0.1, 0.2$, which are depicted by red, blue, and green lines, respectively.

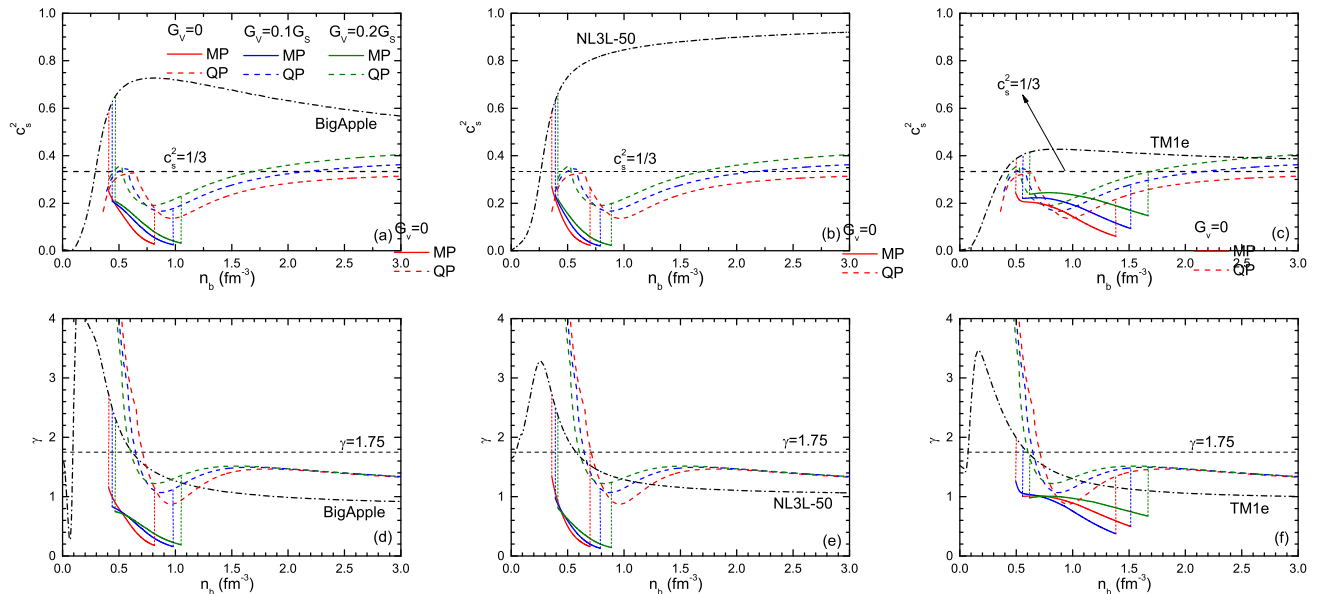


FIG. 2: (Color online) The squared sound velocity c_s^2 (upper panel) and the polytropic index γ (lower panel) as functions of the baryon number density n_b with varying vector coupling $G_V = 0, 0.1, 0.2$. The labels are consistent with those in Fig. 1. Additionally, in the upper panel, a short dash line is utilized to represent the conformal limit with $c_s^2 = 1/3$. $\gamma = 1.75$ in the lower panel, which serve as reference values to distinguish the nucleon degree of freedom from non-nuclear degrees of freedom, is also shown by short dash line. It should be mentioned that the reasonable results of hadronic matter (quark matter) should lie in the low densities (relatively high densities), the expanded results only shown for comparison.

thoroughly investigate the EOS and its impact on the internal structure of the most massive NSs. To describe the hadronic matter, we employ the RMF/RMFL models, while the NJL model with repulsive vector coupling is utilized for quark matter. The hadron-quark mixed phase is treated under the Gibbs equilibrium condition. For the representation of larger mass NSs, we employ the stiff parameter sets BigApple and NL3L-50, while the TM1e parameter set is used to illustrate the results for NSs with a mass around $2 M_\odot$. The results obtained from the NL3 parameter set are included in select figures for comparison purposes, as this set tends to predict excessively large radii and tidal deformability compared to observational data.

In Figure 1, we illustrate the EOSs for the hadronic phase, mixed phase, and quark phase using the BigApple, NL3L-50, and TM1e parameter sets, considering various strengths of vector couplings, $G_V = 0, 0.1, 0.2 G_S$. Before a density of $0.7 fm^{-3}$, the EOS lines for the hadronic phase using the BigApple and NL3L-50 parameter sets exhibit similarities, with BigApple being slightly softer. This shortly delay in the onset of the mixed phase, combined with an enlarged range of the mixed phase for all values of G_V . The softer parameter set, TM1e, further enhances this trend. However, it is noteworthy that the mixed phase EOS derived from TM1e is stiffer compared to that of BigApple and NL3L-50. This observation is counter-intuitive since, despite the hadron-quark phase

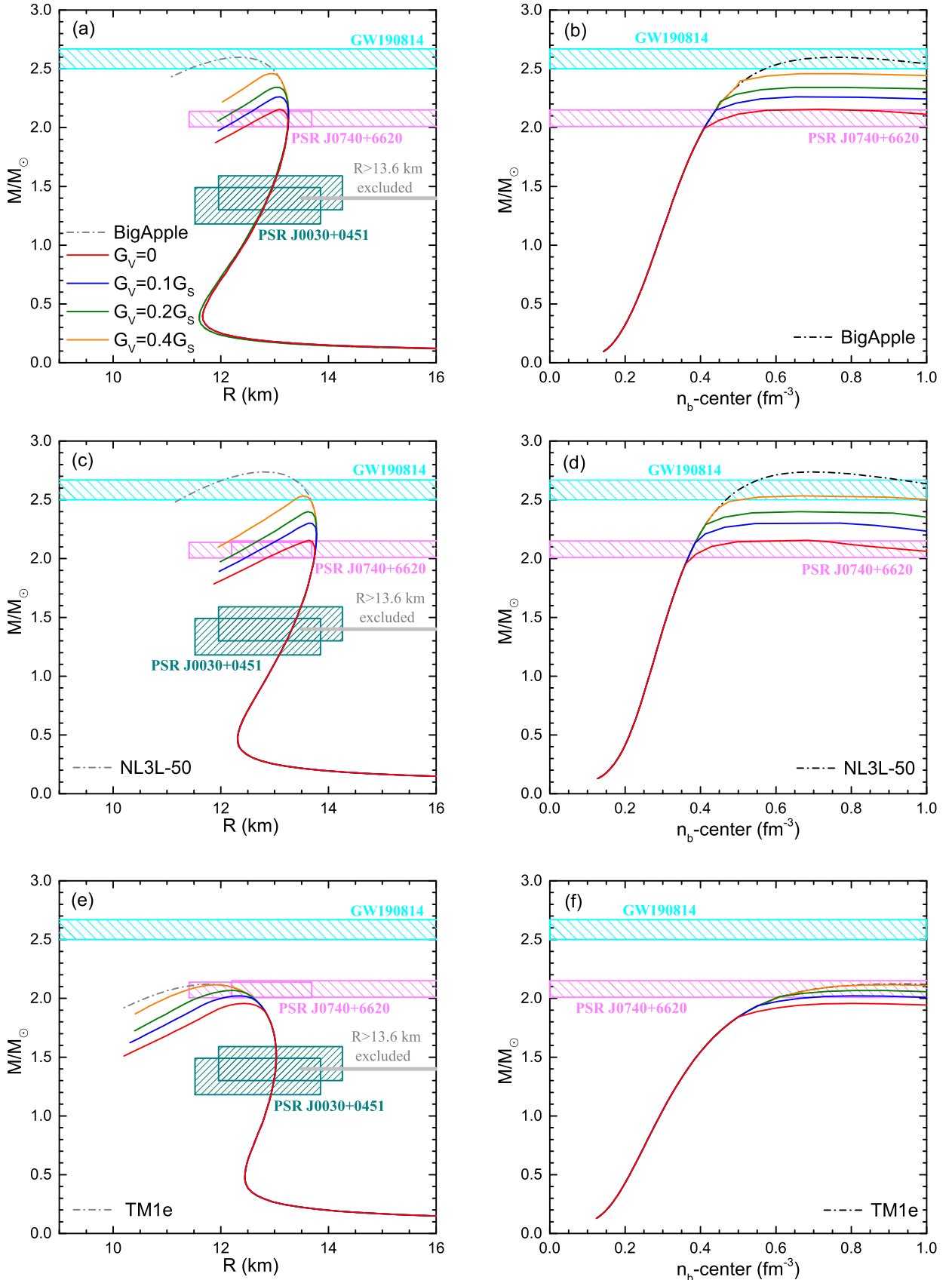


FIG. 3: (Color online) The mass-radius relations (left panel) and mass-central density relations (right panel) of NS with different model parameters. The results from pure hadronic EOS (dash-dot lines) are compared with those including hadron-quark phase transition for different vector couplings. The shaded areas correspond to simultaneous measurements of the mass and radius range from NICER for PSR J0030+0451 [14, 15] and PSR J0740+6620 [16, 17], respectively. The radius constraint $R_{1.4} \leq 13.6$ km is presented with light grey [20]. The hypothesis that the second component of GW190814 is a NS is also denoted [18].

transition being delayed for a softer EOS (TM1e), the stiffness of soft EOS (TM1e) at the onset density of the mixed phase is still lower than that of the stiff EOS (BigApple and NL3L-50). This is illustrated in Figure 2. One plausible hypothesis is that a stiffer hadronic EOS results in higher energy within the mixed phase, causing nucleons to dissociate into quarks more rapidly than in a softer hadronic EOS. Consequently, the rate of soft EOS stiffness change becomes smoother, as evident in Figure 2. With increasing G_V , the onset of the mixed phase shifts to higher densities, accompanied by an increase in the pressure of the mixed phase. The degrees of freedom of the mixed phase encompass those of both the hadronic and quark phases, contributing to the gentlest pressure change among the phases. We utilize the squared sound velocity c_s and the polytropic index γ to quantify the stiffness of EOSs as illustrated in Fig. 1. The sound velocity c_s is defined as $c_s^2 = \partial P / \partial \epsilon$, which asymptotically approaches $1/3$ in the conformal limit corresponding to free mass-less quarks. The conformal limit usually requires $n_b \geq 40n_0$. On the other hand, the polytropic index is defined as $\gamma = d(\ln P) / d(\ln \epsilon)$, and has a value $\gamma = 1$ in conformal limit matter. The squared sound speed (upper panel) and the polytropic index (lower panel) as functions of the baryon number density n_b are depicted in Fig. 2. We show the results that n_b stretched up to 3 fm^{-3} only for comparison purpose where the hadronic matter models used in this study should not applicable at such high densities. Both sound velocity and the polytropic index could characterize the stiffness change of the EOS, but sound velocity is the better choice in low densities because of it without a fluctuation. The decrease of sound velocity of BigApple and TM1e may be related to the effect of parameter Λ_v in RMF models. The sudden decrease in the squared sound velocity c_s^2 or the polytropic index γ at the onset of the mixed phase corresponds to an increase in degrees of freedom. That values of c_s^2 and γ for the mixed phase are the lowest among three phases. Towards the end of the mixed phase, the change trend of c_s^2 close to zero (especially for BigApple and NL3L-50), resembling the results of the Maxwell construction (where $c_s^2 = 0$). This is due to the fact that at the end of the mixed phase in the Gibbs construction, the number density of leptons approaches zero, resulting in the hadronic and quark parts approaching local charge neutrality, similar to the Maxwell construction. The value $\gamma = 1.75$, from Ref. [23], splits the pure nucleon part and non-nucleon part: all the hadronic matter EOS have $\gamma > 1.75$ except the case TM1e- $G_V = 0.2 G_S$, and all the mixed phase and quark phase EOSs have $\gamma < 1.7$.

In Fig. 3, we display the mass-radius relations (left panel) and mass-central density relations (right panel) for BigApple, NL3L-50 and TM1e EOSs with different strength of vector coupling $G_V = 0, 0.1, 0.2, 0.4 G_S$. Several constraints from astrophysical observations are also displayed in different color regions. The predicted maximum mass of HS depends on G_V . Due to the stiff enough EOS of hadronic matter, even with $G_V = 0$ Bi-

gApple and NL3L-50 could support a maximum mass of $M_{\text{max}} \sim 2.0 M_\odot$, while TM1e requires $G_V \geq 0.1 G_S$. The maximum mass could reach $2.5 M_\odot$ with $G_V \geq 0.4 G_S$ using the NL3L-50 parameter set. The appearance of quark degrees of freedom in the mixed phase leads to an obvious reduction of the maximum mass of NS, but larger values of G_V make the reduction of maximum mass smaller. Compared with stiffer EOSs (BigApple and NL3L-50), the effect of different values of G_V on TM1e is smaller. The normal $1.4 M_\odot$ NS properties are determined by the EOS around $2 n_0$, where quarks have not appeared. Therefore, the mixed phase does not affect mass-radius line through PSR J0030+0451 constraints [14, 15]. Even when considering the hadron-quark phase transition, the radius and mass of NSs are still mainly effected by the hadronic part. A large enough mixed phase core in the maximum mass NS is expected, but with $M \sim 2 M_\odot$ the mixed phase core is not supported by these parameter sets in this study, except for TM1e- $G_V = 0.1 G_S$.

To better examine the properties of the maximum mass NS, we present the relations of mass and radius of the maximum mass NS in Fig. 4. The solid square indicates where the deconfined quarks appear. On the left side of the solid square are the mixed phase core, which could close to 6 km and around $0.3 M_\odot$ for $G_V = 0$. With larger G_V , stiffer quark matter EOS, leading the size and mass of the mixed-phase core of the maximum mass NS decrease. A relative softer hadronic phase EOS (TM1e) could have relative large size and mass of the mixed phase core compared with stiffer hadronic phase EOS (BigApple and NL3L-50), though offers relative small maximum mass. No pure quark core is observed under the framework in this study, as the pure quark phase onset density is beyond the maximum mass NS center density, as seen in Fig. 3 (right panel). Fig. 5 shows the central density-radius relation of maximum mass NS, including the NL3 parameter set, which offers a larger mixed phase radius than others. This is because the NL3 parameter set predicts larger radius than other parameter sets for all mass values, but beyond the observation constraints. With $G_V = 0$, around $1/3 - 1/2$ radius of the maximum mass NS are the mixed phase.

The relation between maximum value of squared speed of sound $\max(c_s^2)$ and the radius of the mixed phase of the maximum mass NS R_{MP} is exhibited in Fig. 6. The $\max(c_s^2)$ is actually corresponds to the c_s^2 at density $n_b(1)$ for hadronic matter, $\max(c_s^2) = c_{s,HP}^2(n_b(1))$, as shown in Fig. 2. But the extreme case where $R_{\text{MP}} = 0$, with no mixed phase core, $\max_{c_s^2} = c_{s,HP}^2(n_c)$, as shown in 7, where the central density of the maximum mass NS little than the onset density of the mixed phase. Because $n_b(1)$ is affected by G_V , within the same model, $\max(c_s^2)$ and $n_b(1)$ both increase with G_V increase, together with R_{MP} decrease, leading to a smaller proportion of the mixed phase radius in the maximum mass NS. This trend is consistent with the findings in Ref [23].

We examined the effect of vector coupling on the phase

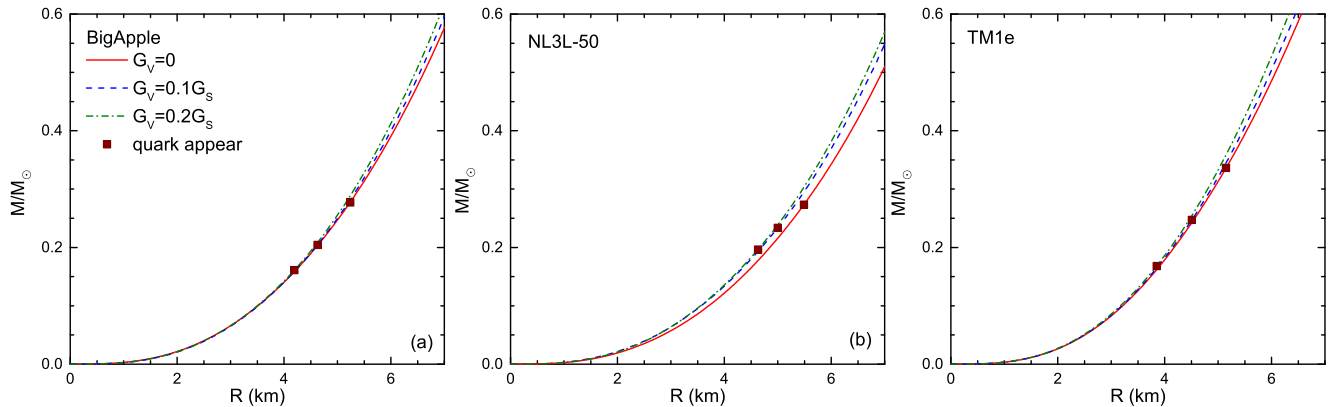


FIG. 4: (Color online) Mass-radius relations for the maximum mass NS. The solid square indicates where the quark appears.

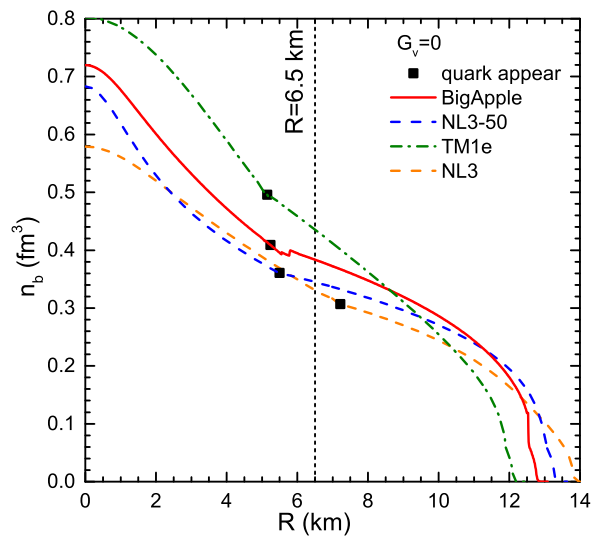


FIG. 5: (Color online) Central-density n_b and radius R relations of the maximum mass NS with $G_V = 0$. The line $R = 6.5$ km represents approximately half the radius of the entire NS.

transition density and maximum mass NS central density n_c , as shown in Fig. 7. With G_V increase, the mixed phase is delayed to higher densities, affecting both $n_b(1)$ and $n_b(2)$, but leaving the central density n_c relatively stable. If $n_c < n_b(1)$, it indicates that the maximum stable density occurs in the pure hadronic matter without deconfined quarks. The maximum mass is primarily determined by the stiffness EOS of the hadronic phase, whose range is influenced by vector coupling G_V . However, a strong enough G_V can prevent the hadron-quark phase transition, and the threshold value of c is

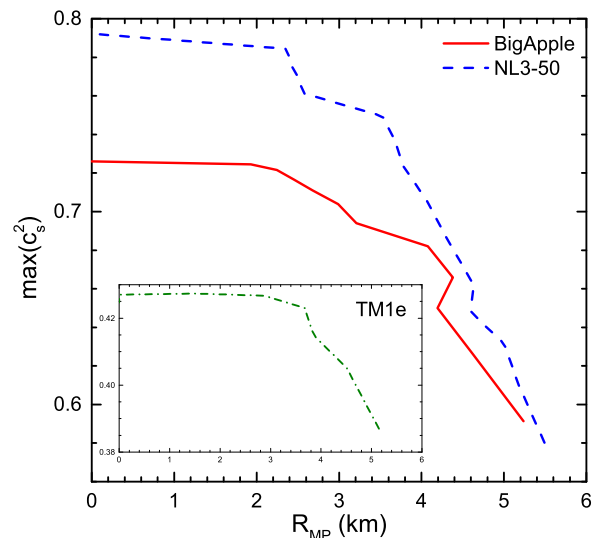


FIG. 6: (Color online) The relations between the radius of the mixed phase R_{MP} and the maximum squared sound velocity $\max(c_s^2)$ of the maximum mass NS. The units of the inside picture are same as those in the outside.

determined by the EOS of hadronic phase. BigApple and NL3L-50 support a maximum G_V value of about $G_V < 1.1 G_S$ and $G_V < 1.2 G_S$, respectively. Through this idea, TM1e supports a maximum G_V value about $G_V < 0.55 G_S$, however, with $G_V \sim 0.4$, $n_b(2)$ is larger than 2.0 fm^{-3} , which is over 15 times the saturation density n_0 . Therefore, ~ 0.4 could consider as the threshold value. The relatively large upper limit derived here benefits the stiffness of the EOS. This, coupled with the results from Fig. 2 showing that larger values of G_V lead to larger c_s^2 , which should not exceed $1/3$ at high densi-

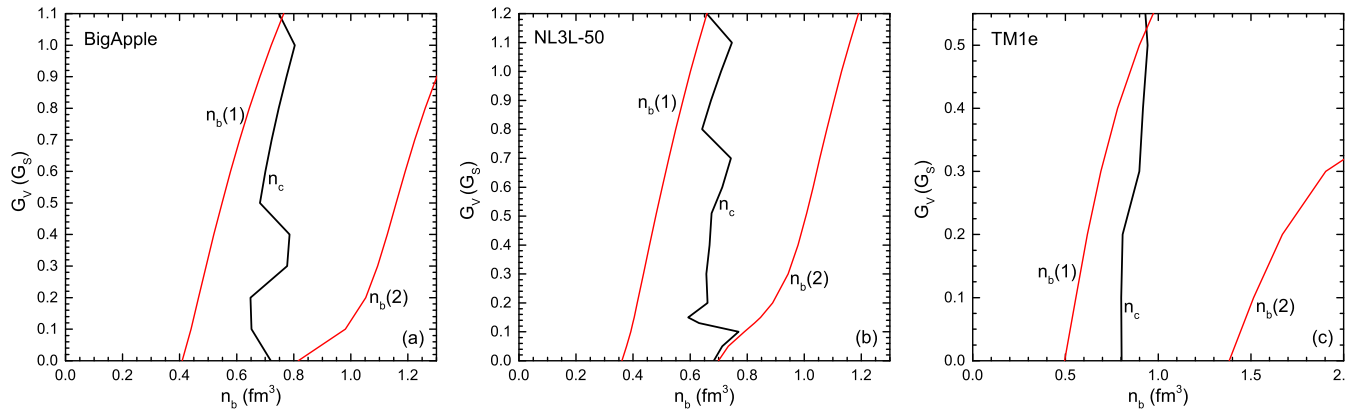


FIG. 7: (Color online) The phase transition density $n_b(1)$, $n_b(2)$ and the center density of the maximum mass NS n_c as a function of baryon number density n_b with different value of G_V .

ties, leads to the universal conclusion that non-zero G_V should be density-dependent. The decrease in the range between $n_b(1)$ and n_c as G_V increase indicates a reduction in the mixed phase range. Beyond the threshold value of G_V , though the hadron-quark phase transition could occur, the mixed phase is not supported in a NS. With given G_V , compared with results of NL3L-50, $n_b(1)$ derived from BigApple slightly moves to higher density, but $n_b(2)$ shifts more. This can also explained by the nucleons dissociation rate hypothesis above that nucleons with NL3L-50 dissociate faster to quarks than with BigApple interaction.

IV. SUMMARY

In this work, we focus on exploring the properties of maximum mass neutron stars with quark degrees of freedom. We have conducted an investigation of the EOS with the hadron-quark phase transition under Gibbs equilibrium. To achieve this, we have employed the RMF/RMFL model to characterize hadronic matter, while the NJL model with repulsive vector coupling has been utilized for the representation of quark matter. Our findings indicate that the properties of maximum mass NSs are significantly influenced by the model parameters used, including the strength of the vector coupling. Specifically, a stiffer hadronic matter EOS and a larger vector coupling are shown to potentially support more massive NSs. The presence of vector coupling has the capacity to increase the maximum mass of neutron stars, mitigating the reduction in maximum mass caused by the appearance of quarks to a certain extent. However, no

clear correlation has been observed between the central density of maximum mass NSs and the vector coupling. Under the condition of the same vector coupling strength G_V , a relatively softer hadronic matter EOS has the potential to support a relatively larger mixed phase core. This core could occupy nearly half of the entire neutron star when $G_V = 0$, but the corresponding mass of the mixed phase core is comparatively small in relation to the total mass.

In summary, our study reveals that the global properties of maximum mass NSs are sensitive to the strength of the maximum sound velocity of the EOS. Furthermore, it is possible for a relatively large radius of the mixed phase to exist in the core of maximum mass NSs when there is a small vector coupling in the quark matter. But for NSs have $M \sim 2 M_\odot$, only tiny mixed phase core is possible in this study (with $\text{TM1e-}G_V \simeq 0.1G_S$). If the vector coupling is sufficiently large to exceed a certain threshold, it can prevent the occurrence of the hadron-quark phase transition in NSs. Besides, a non-zero G_V should be density dependent to fulfil the sound speed conformal limit.

Acknowledgment

This work is supported by the National Natural Science Foundation of China under Grants No. 12305148, No. 11975132, No. 12205158, Hebei Natural Science Foundation No. A2023203055, and the Shandong Provincial Natural Science Foundation, China under Grants No. ZR2023QA112, No. ZR2022JQ04, No. ZR2021QA037, and No. ZR2019YQ01.

[1] G. Baym, T. Hatsuda, T. Kojo, P. D. Powell, Y. Song and T. Takatsuka, Rep. Prog. Phys. **81**, 056902 (2018).

[2] G. Baym and S. A. Chin, Phys. Lett. B **62**, 241–4 (1976).

- [3] N. K. Glendenning, *Phys. Rev. D* **46**, 1274 (1992).
- [4] Witten E., *Phys. Rev. D*, **30**, 272 (1984).
- [5] H. Liu, Y.-H. Yang, Y. Han, and P.-C. Chu, *Phys. Rev. D* **108**, 034004 (2023).
- [6] N. K. Glendenning, *Phys. Rep.* **342**, 393 (2001).
- [7] F. Weber, *Prog. Part. Nucl. Phys.* **54**, 193 (2005).
- [8] L. Brandes, W. Weise, and N. Kaiser, *Phys. Rev. D* **108**, 094014 (2023).
- [9] E. Fonseca, H.T. Cromartie, T.T. Pennucci, et al., *Astrophys. J. Lett.* **915** L12 (2021).
- [10] H. T. Cromartie, E. Fonseca, S. M. Ransom, et al., *Nat. Astron.* **4**, 72 (2020).
- [11] Z. Arzoumanian et al., *Astrophys. J. Suppl.* **235**, 37 (2018).
- [12] J. Antoniadis, P. C. C. Freire, N. Wex, et al., *Sci*, **340**, 448 (2013).
- [13] R.W. Romani, D. Kandel, A.V. Filippenko, T.G. Brink, W. Zheng, *Astrophys. J. Lett.* **934**, L18 (2022).
- [14] T. E. Riley et al., *Astrophys. J. Lett.* **887**, L21 (2019).
- [15] M. C. Miller et al., *Astrophys. J. Lett.* **887**, L24 (2019).
- [16] T. E. Riley, A. L. Watts, P. S. Ray, et al., *Astrophys. J. Lett.* **918**, L27 (2021).
- [17] M. C. Miller, F. K. Lamb, A. J. Dittmann, et al., *Astrophys. J. Lett.* **918**, L28 (2021).
- [18] R. Abbott et al. (LIGO Scientific and Virgo Collaborations), *Astrophys. J. Lett.* **896**, L44 (2020).
- [19] B. P. Abbott, et al. (The LIGO Scientific Collaboration and the Virgo Collaboration) *Phys. Rev. Lett.* **119**, 161101 (2017).
- [20] E. Annala, T. Gorda, A. Kurkela, A. Vuorinen, *Phys. Rev. Lett.* **120**, 172703 (2018).
- [21] M. Ferreira, R. C. Pereira, and C. Providência, *Phys. Rev. D* **103**, 123020 (2021).
- [22] H. Liu, X. -M. Zhang and P.-C. Chu, *Phys. Rev. D* **107**, 094032 (2023).
- [23] E. Annala, T. Gorda, A. Kurkela, J. Nättilä, A. Vuorinen, *Nat. Phys.* **16**, 907 (2020).
- [24] M. G. Alford, S. Han, and K. Schwenzer, *J. Phys. G* **46**, 114001 (2019).
- [25] A. Bauswein, N. F. Bastian, D. B. Blaschke, K. Chatziioannou, J. A. Clark, T. Fischer, and M. Oertel, *Phys. Rev. Lett.* **122**, 061102 (2019).
- [26] Y. J. Huang, L. Baiotti, T. Kojo, K. Takami, H. Sotani, H. Togashi, T. Hatsuda, S. Nagataki, and Y. Z. Fan, *Phys. Rev. Lett.* **129**, 181101 (2022).
- [27] J. J. Li, A. Sedrakian, and M. Alford, *Phys. Rev. D* **104**, L121302 (2021).
- [28] S. Podder, S. Pal, D. Sen, G. Chaudhuri, *Nucl. Phys. A* **1042**, 122796 (2024).
- [29] J. J. Li, A. Sedrakian, and M. Alford *Astrophys. J.* **944**, 206 (2023).
- [30] W. M. Spinella, A Systematic Investigation of Exotic Matter in Neutron Stars, Ph.D. thesis, Claremont Graduate University & San Diego State University (2017).
- [31] X. H. Wu, S. S. Bao, H. Shen, and R. X. Xu, *Phys. Rev. C* **104**, 015802 (2021).
- [32] T. Maruyama, S. Chiba, H.J. Schulze, T. Tatsumi, *Phys. Lett. B* **659**, 192 (2008).
- [33] X. H. Wu and H. Shen, *Phys. Rev. C* **99**, 065802 (2019).
- [34] F. J. Fattoyev, C. J. Horowitz, J. Piekarewicz, and B. Reed, *Phys. Rev. C* **102**, 065805 (2020).
- [35] S. S. Bao, J. N. Hu, Z. W. Zhang, and H. Shen, *Phys. Rev. C* **90**, 045802 (2014).
- [36] X. H. Wu, A. Ohnishi, and H. Shen, *Phys. Rev. C* **98**, 065801 (2018).
- [37] G. A. Lalazissis, J. König and P. Ring, *Phys. Rev. C* **55**, 540 (1997).
- [38] I. Tews, J. M. Lattimer, A. Ohnishi, and E. E. Kolomeitsev, *Astrophys. J.* **848**, 105 (2017).
- [39] B. A. Li, B. J. Cai, W. J. Xie, and N. B. Zhang, *Universe* **7**, 182 (2021).
- [40] N. Yasutake, R. Lastowiecki, S. Benić, D. Blaschke, T. Maruyama, and T. Tatsumi, *Phys. Rev. C* **89**, 065803 (2014).
- [41] K. Masuda, T. Hatsuda, and T. Takatsuka, *Astrophys. J.* **764**, 12 (2013); *Prog. Theor. Exp. Phys.* **7**, 073D01 (2013).
- [42] P. C. Chu, X. Wang, L. W. Chen, and M. Huang, *Phys. Rev. D* **91**, 023003 (2015).
- [43] R. C. Pereira, P. Costa, and C. Providência, *Phys. Rev. D* **94**, 094001 (2016).
- [44] P. Rehberg, S. P. Klevansky, and J. Hüfner, *Phys. Rev. C* **53**, 410 (1996).